Journal of Geophysical Research: Space Physics

RESEARCH ARTICLE
10.1029/2018JA025496

Key Points:
- This study delineates the effects of flare and storm time electric fields over the low-latitude ionosphere during 6 to 8 September 2017
- The role of center-to-limb distance of active region 12673 in changing *E* and *F*-region densities during X9.3 flare on 6 September is assessed
- Storm time PPE field and composition changes caused significant low-latitude TEC enhancements, while the similar was absent at the equator

Supporting Information:
- Supporting Information S1

Correspondence to:
M. S. Bagiya,
bagiyamala@gmail.com;
mala@iigs.iigm.res.in

Citation:
Bagiya, M. S., Thampi, S. V., Hui, D., Sunil, A. S., Chakrabarty, D., & Choudhary, R. K. (2018). Signatures of the solar transient disturbances over the low latitude ionosphere during 6 to 8 September 2017. *Journal of Geophysical Research: Space Physics*, *123*, 7598–7608. https://doi.org/10.1029/2018JA025496

Received 20 MAR 2018
Accepted 2 AUG 2018
Accepted article online 11 AUG 2018
Published online 6 SEP 2018

Signatures of the Solar Transient Disturbances Over the Low Latitude Ionosphere During 6 to 8 September 2017

Mala S. Bagiya[1], Smitha V. Thampi[2], Debrup Hui[1], A. S. Sunil[1], D. Chakrabarty[3], and R. K. Choudhary[2]

[1]Indian Institute of Geomagnetism (DST), Navi Mumbai, India, [2]Space Physics Laboratory, Vikram Sarabhai Space Centre, Thiruvananthapuram, India, [3]Physical Research Laboratory, Ahmedabad, India

Abstract Low latitude ionospheric behavior during solar transient disturbances of solar flares and storm time penetrating electric fields comprises an important part of the Earth's space weather. The flares enhance the electron density of the sunlit ionosphere by supplying excess solar radiation. However, the degree of these density changes is subjective if a geomagnetic storm persists simultaneously. The present case study addresses the ionospheric variations over the Indian longitudes under the combined effects of the solar flares and a geomagnetic storm during 6 to 8 September 2017 and probably the first of its kind in delineating the effects of these two over the low latitude ionosphere. The X9.3 class flare of 6 September, which occurred during non-storm conditions, produced an intense *E* region ionization (~500% over the ambient). However, the total electron content response to this flare was comparatively weak. The flares on 7 and 8 September occurred during the 7–8 September geomagnetic storm. Though the 8 September flare occurred with higher intensity (M8.1) and early in local time compared to the flare of 7 September (M7.3), the equatorial electrojet current enhancement was lesser on 8 September (~75% over the ambient) than that of 7 September (~110% over the ambient). This aspect is discussed in view of the storm time convection effects over the low latitudes during 7–8 September storm. The total electron content did not respond to the flares of 7 and 8 September. This behavior is attributed to the varying center-to-limb distance of the solar active region 12673 during this period.

1. Introduction

Low latitude ionospheric *E* and *F* regions respond varyingly to solar disturbances like solar flares and coronal mass ejections, which is an important element of our space weather. Sudden enhancement in solar radiation in terms of solar flares increases the ionospheric electron density on various scales depending on the severity of the flare. The flare associated X-ray flux produces excess ionization in the ionospheric *D* region, which is primarily responsible for the short radio wave fade-outs, phase, and frequency change of the radio wave and thus adversely affects the wave propagation (e.g., Davies, 1990; Donnelly, 1976; Mitra, 1974; Thome & Wagner, 1971). The soft X-ray (0.8–20 nm) in addition to extreme ultraviolet (EUV) flux (79.6–102.7 nm) ionizes the *E* region and thus affects the *E* region current system (e.g., Chakrabarty et al., 2013; Nagata, 1966; Raja Rao & Panduranga Rao, 1963; Rastogi et al., 1999; Richmond & Venkateswaran, 1971). The *F* region responds profoundly to the solar radiation in the EUV range of 17 to 91.1 nm (e.g., Liu et al., 2006; Mahajan et al., 2010; Mendillo et al., 1974; Tsurutani et al., 2005). Various studies have emphasized that the impact of solar X-ray and EUV fluxes during flare events varies with the center-to-limb distance of the active region (i.e., origin of the flare) (e.g., Donnelly, 1976; Le et al., 2011; Leonovich et al., 2010; Mahajan et al., 2010; Tsurutani et al., 2005; Zhang et al., 2011, and references therein).

Most of the studies on ionospheric response to solar flares pertain to periods during which either the effects of geomagnetic storms were not yet prevailed or the flare events were not accompanied by geomagnetic storms. The effects of geomagnetic storms over low-latitude ionosphere can be understood through electrodynamic (penetration of storm induced electric fields) and neutral dynamic (storm induced thermospheric neutral composition changes) coupling between high and low latitude ionosphere (e.g., Bagiya et al., 2011, 2014, 2018; Blanc & Richmond, 1980; Fejer et al., 1983; Kelley et al., 2003; Nishida, 1968; Prolss, 1997; Tsurutani et al., 2004, and references therein). Both the flare and storm induced ionospheric changes vary with the local time (e.g., Bagiya et al., 2011; Chakrabarty et al., 2013).

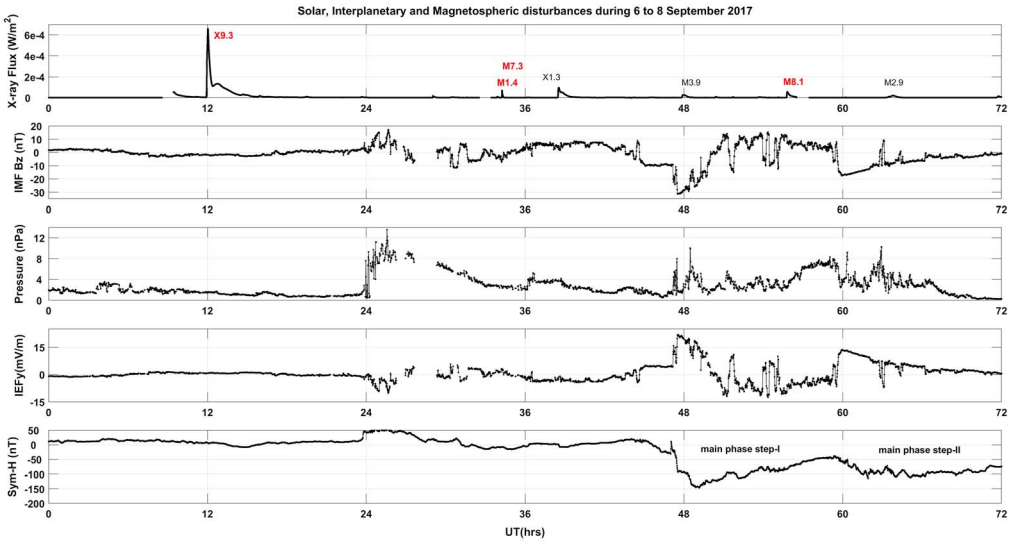

Figure 1. Variations in solar (X-ray irradiance), interplanetary (IMF B_z, solar wind pressure, and IEF_y) and magnetospheric (SYM-H) parameters during 6 to 8 September 2017. The major solar flares during this period are labeled with the respective flare intensity. The flares highlighted in red labels are considered for this study. IMF = interplanetary magnetic field; IEF = interplanetary electric field.

The present study aims to understand the low latitude ionospheric variations under the combined effects of the excess solar radiation during solar flares and storm time transient electric fields, a topic which has not been addressed extensively so far. As mentioned the low latitude ionospheric responses to flares and storms have been studied independently in detail, the present attempt is exclusive in delineating the effects of these two over the low latitude ionosphere. We believe that the solar disturbances in terms of multiple major solar flares during 6 to 8 September 2017 and a geomagnetic storm on 7–8 September 2017 could be considered as ideal scenario to improve our understanding on their interwoven effects on the low latitude ionosphere. For this study, we analyze the equatorial electrojet (EEJ) current and Global Positioning System (GPS)-total electron content (TEC) observations at the Indian longitudes during 6 to 8 September 2017. The varying degree of ionization changes as observed through the EEJ current and the GPS-TEC during multiple intense flares is discussed in terms of the active region location (from where the flares have emerged) over the solar disk, the local time occurrence of the flares (i.e., solar zenith angle variations), and the storm time transient electric fields. Moreover, this case study compares the flare induced EEJ current enhancements during the 7–8 September geomagnetic storm to bring out the role of storm time convection in manifesting these enhancements.

2. Data and Methodology

Figure 1 presents the X-ray irradiance (0.1 to 0.8 nm) derived from Geostationary Operational Environmental Satellite (GOES)-15 along with interplanetary and magnetospheric parameters during 6 to 8 September 2017. GOES-15 is a geostationary satellite parked at 135°W longitude. The GOES-15 Space Environment Monitor suite has multiple instruments to measure the radiation in the X-ray and EUV band, in situ particle flux, and magnetic field. The GOES X-ray sensor gives X-ray flux in the wavelength range of 0.05 to 0.4 and 0.1–0.8 nm (Hanser & Sellers, 1996). The remaining parameters in Figure 1, provided by the National Aeronautics and Space Administration (NASA) Coordinated Data Analysis (CDA) database (http://cdaweb.sci.gsfc.nasa.gov/), include north-south component of interplanetary magnetic field (IMF B_z), solar wind pressure (P_{SW}), dawn-dusk component of interplanetary electric field (IEF_y), and the symmetric ring current (SYM-H) index, which depicts the ring current activity during this period. Further details about the data specifications can be found in the CDA website. The 1-min average values for the above mentioned parameters have been used for this analysis. Multiple flares are evident from the X-ray irradiance observations during 6 to 8 September, while the interplanetary and ring current parameters show the presence of a geomagnetic storm during 7 to 8 September. The major solar flares during 6 to 8 September are labeled with their respective

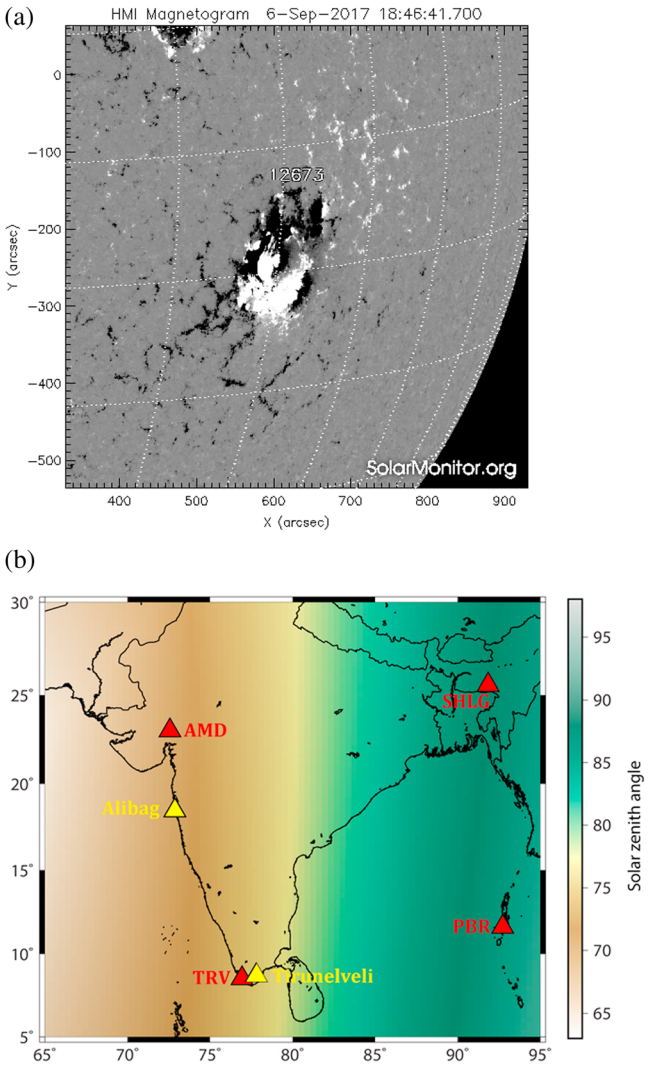

Figure 2. (a) Magnetogram of the Sun's surface showing the active region 12673 on 6 September 2017. The magnetogram was recorded by Helioseismic and Magnetic Imager on board Solar Dynamic Observatory (courtesy: NASA). (b) Locations of GNSS receivers over the Indian region are shown with red triangles. The yellow triangles show the locations of magnetometer stations used to derive equatorial electrojet. The variations of solar zenith angle over the Indian region at the occurrence time of X9.3 flare at ~11:53 UT on 6 September are shown as the colored background.

intensities in the figure. The flares highlighted with red labels occurred during daytime over the Indian region and therefore are considered for this study. From the SYM-H variations (Figure 1), it could be stated that the storm of 7–8 September 2017 also had two-step main phase as similar to the strongest storm of the solar cycle 24 till date, which occurred on 17 March 2015 (e.g., Bagiya et al., 2017; Kamide & Kusano, 2015). The slow storm recovery started on 8 September and persisted till 9 September as exhibited by the SYM-H (not shown in the figure). Due to lack of interplanetary parameters on 9 September, we will not discuss any ionospheric variations on this day.

As mentioned, we present here EEJ current and GPS-TEC observations at the Indian longitudes to study the response of low latitude ionosphere to these various solar disturbances. EEJ shows the equatorial *E* region current strength and is derived from the deviation in the horizontal north-south magnetic field component (ΔH) measured at the off-equatorial ground station to that of the equatorial station (e.g., Rastogi & Klobuchar, 1990). The ΔH observations from Alibag (18.46°N, 72.87°E; magnetic latitude 10.19°N) and Tirunelveli (8.70°N, 77.80°E; magnetic latitude 0.03°N) are used to derive the EEJ strength ($\Delta H_{(\text{Tirunelveli})} - \Delta H_{(\text{Alibag})}$) during both solar disturbed and quiet conditions. We present the disturbed time EEJ current perturbations along with the mean of five quiet days' EEJ observations of 22 to 26 September 2017. These quiet days are among the 10 quietest days of the month as listed by World Data Center, Kyoto.

The GPS-TEC is one of the powerful tools to study the *F* region electron density variations during both solar quiet and disturbed conditions (e.g., Rama Rao et al., 2006; Bagiya et al., 2011, 2009, and references therein). TEC is the integrated electron density along the line of sight of satellite to a receiver and considered to be mainly weighted by the *F* region ionization density. We have extracted slant GPS-TEC data from multi-institute's Global Navigation Satellite System (GNSS) receivers located over the India during 6 to 8 September 2017. These receivers can record multifrequency signals from global navigation satellite constellations and facilitate the continuous ionospheric monitoring during solar quiet and disturbed conditions. The typical receiver setup samples the phase and amplitude at 50-Hz output rate at given frequency band for all satellites, which are in the field-of-view of the antenna and compute the TEC and scintillation index. The locations of both ground magnetic field and TEC observable stations are shown in Figure 2a and also listed in Table 1 along with the respective responsible institutes for quick reference. The elevation cutoff of ~20° is applied to TEC data in order to reduce the multipath effect. The slant TEC is further converted to vertical TEC using the method suggested by Klobuchar (1986). The vertical TEC is referred as TEC henceforth. The storm time TEC is presented along with the average of three quietest days TEC of 22 to 24 September 2017. The selection of these 3 days is based on the common availability of GPS-TEC observations from all four stations. In addition to the station locations, Figure 2b indicates the variations of solar zenith angle at ~11:53 UT on 6 September over the Indian longitudes shown by the colored background. This aspect will be discussed later in the text.

The EUV in the wavelength range of 17 to 91.1 nm is the major radiation, which ionizes the *F* region; thus, we have looked into EUV irradiance measured in the wavelength range of 27.16–33.8 nm (centered around 30 nm) using Extreme Ultraviolet Spectro-Photometer (ESP) on board Solar Dynamic Observatory (SDO). SDO is a geosynchronous satellite dedicated to observe the Sun and is parked at 102°W (Pesnell et al.,

Table 1
TEC and Ground Magnetic Field Observable Station Locations and Respective Responsible Institutes

GNSS receiver station (code)	Latitude (N)	Longitude (E)	Responsible institute
Portblair (*pbri*)	11.62°	92.73°	Indian Institute of Geomagnetism, India
Shillong (*shlg*)	25.55°	91.85°	Indian Institute of Geomagnetism, India
Trivandrum (*trv*)	8.52°	76.94°	Space Physics Laboratory, VSSC, India
Ahmedabad (*amd*)	23.02°	72.57°	Physical Research Laboratory, India
Magnetometer station			
Tirunelveli	8.7°	77.8°	Indian Institute of Geomagnetism, India
Alibag	18.46°	72.87°	Indian Institute of Geomagnetism, India

2012). ESP measures solar irradiance in five different wavelength ranges. The EUV data are presented in the next section.

3. Results

The period of 6 to 8 September 2017 contained multiple intense solar flares including the X9.3 class flare —the strongest flare of this decade occurred on 6 September. The NASA SDO marked the origin of these flares as active region 12673. Figure 2a shows the location of this region over the solar disk on 6 September. While transiting towards the limb over the solar disk, this active region acquired a complex magnetic configuration and ejected a series of intense flares between 6 to 8 September (*source:* www.space-weather.com).

Figure 3 shows the low latitude ionospheric changes during the X9.3 flare on 6 September. The EEJ current observations are presented in Figure 3a along with the X-ray irradiance (0.1 to 0.8 nm). The flare onset is at ~11:54 UT in X-ray, and an intense peak occurred at ~12:02 UT. The EEJ current shows two prominent peaks at ~9:12 and ~12:02 UT. Due to lack of X-ray flux during the first EEJ peak at ~9:12 UT, it is not possible to discuss EEJ current variations during this period. It is important to note that the peak of the X9.3 flare is accompanied by a significant increase in EEJ current. The vertical dashed line shows the time synchronization between the onset of flare and EEJ current response. In order to view this variation in terms of local time, time corresponding to 75°E meridian is given at the top of each panel. The EEJ current is enhanced by ~500% (over the preflare EEJ current value) at ~12:02 UT. It has to be noted that this UT coincided with the local evening hours over the Indian region.

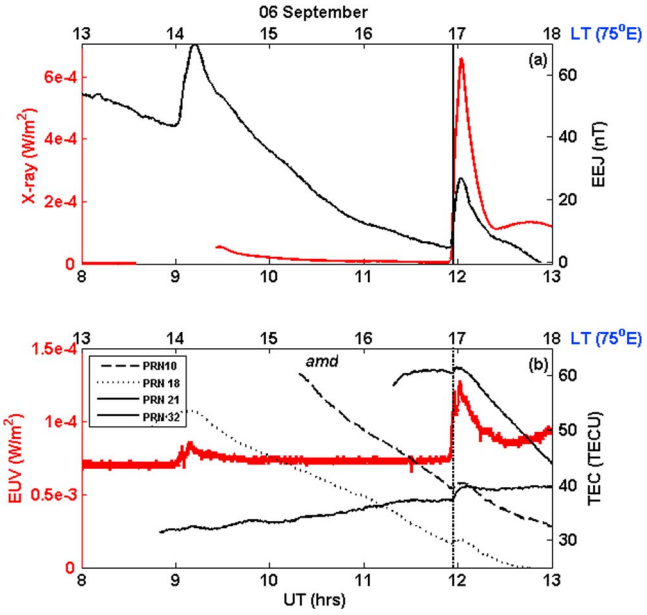

Figure 3. (a) X-ray irradiance (0.1 to 0.8 nm) derived from GOES-15 (red solid line) along with the EEJ current estimated over the Indian region (black solid line) during the occurrence period of X9.3 flare on 6 September (b) EUV irradiance (27.16 to 33.8 nm, centered around 30 nm) as measured using ESP on board SDO (red solid line) along with TEC as recorded by multiple PRNs from *amd* station during the X9.3 flare. Both the universal and local (along 75°E meridian) times are shown in the figure. The time synchronization of flare onset and ionospheric response is presented with vertical dashed black line.

The TEC response to this flare is investigated using the observations from four GPS receiver stations located over the Indian longitudes (Figure 2b and Table 1). Multiple GPS satellites, with different pseudo random number (PRN), as observed from *amd* station recorded TEC increase of ~7% (over the preflare TEC value) following the flare occurrence at ~12:00 UT (Figure 3b). No such TEC variations were observed during the flare at ~9:12 UT. The TEC as recorded from *tvm* GPS station (~4°E from the *amd*) exhibited almost similar magnitude of enhancement following the X9.3 flare (Figure S1 in the supporting information). In Figures 3b and S1, the TEC are presented along with the ESP measured EUV radiation (27.16 to 33.8 nm). It could be observed that EUV radiation also enhanced significantly along with the X9.3 flare onset. It is important to note that IEF_y and SYM-H both did not show any significant change during the X9.3 flare commencement (Figure 1). Thus, the observed EEJ current and TEC variations at ~12:00 UT on 6 September are merely due to the X9.3 flare. It is important to note that the TEC as recoded

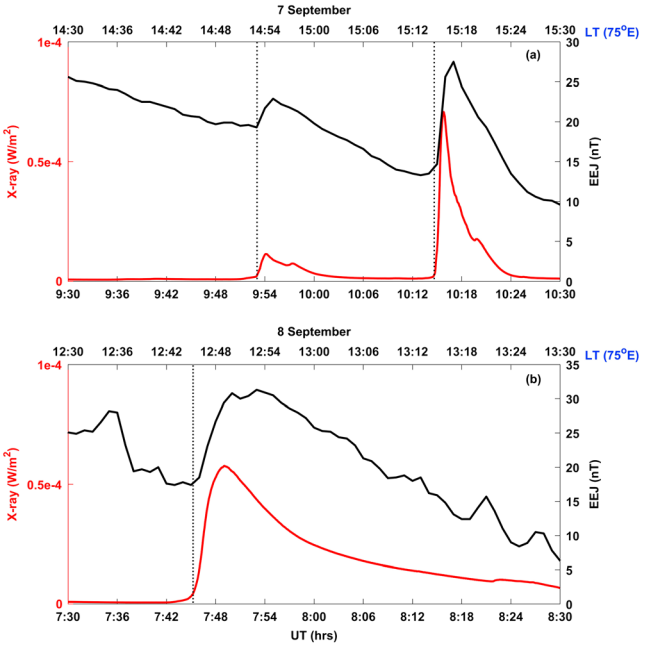

Figure 4. (a) X-ray irradiance along with EEJ current variations during M7.3 flare on 7 September (b) X-ray irradiance along with EEJ current during the flare of M8.1 on 8 September. The variations are presented both in universal as well as local (along 75°E meridian) times. The vertical dashed black line in each figure shows the onset of flares and the initiation of respective EEJ current variations.

from *pbri* and *shlg* GPS stations did not respond to the X9.3 flare and thus not shown here. The active region 12673 ejected multiple intense flares on 7 September. We concentrate here on the two M-class flares of M1.4 and M7.3, which occurred at ~09:49 and ~10:11 UT, respectively, due to their occurrence times, which coincided with the daytime over the Indian longitudes. The EEJ observations during both these flares are shown in Figure 4a along with the X-ray irradiance. The EEJ current responded well to both the flares, and the response was more intense during the M7.3 flare (Figure 4a). The dotted vertical lines show the accordance between the *E* region current variations and the onsets of the flares.

The IMF B_z started fluctuating at ~23:53 UT on 6 September. However, SYM-H did not exhibit any major storm activity until southward IMF B_z intensification at ~23:10 UT on 7 September. It could be noticed that significant IEF_y fluctuations were observed during the occurrence of M1.4 and M7.3 flares on 7 September. The EEJ current variations along with the IEF_y on 7 September are presented separately in Figure 5a for better comparison. The occurrence period of both the flares is highlighted in the figure. It could be noticed that the EEJ current exhibited noteworthy modulations following the IEF_y variations. Despite this, the flare-induced EEJ current variations are very clear on 7 September. This could be verified by its occurrence time synchronization with the onset of the respective flares (Figure 4a). The EEJ current enhanced by ~20% (over the respective preflare EEJ current value) during M1.4 flare, while it enhanced by ~110% (over the respective preflare EEJ current value) during M7.3 flare. Regarding TEC during the above listed M-class flares, no clear TEC variations were observed during these periods.

The sharp increase in southward IMF B_z at ~23:10 UT on 7 September was followed by the main phase initiation for the 7–8 September geomagnetic storm. The maximum SYM-H value, during this storm, was ~−146 nT at ~11:10 UT on 8 September. The solar and interplanetary parameters between 00:00 and

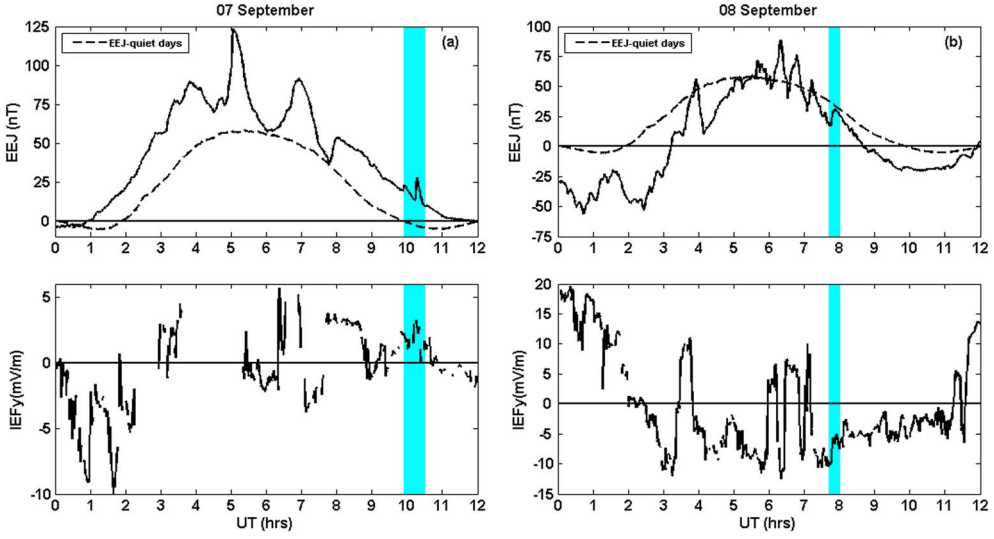

Figure 5. EEJ current during 00:00 to 12:00 UT (dayside over the Indian region) and IEF_y on (a) 7 September and (b) 8 September 2017. EEJ current of the respective days is presented with five quiet days' EEJ current mean from the same month. The highlighted EEJ enhancements are observed in accordance with the flares on 7 and 8 September 2017, respectively. The simultaneous IEF_y variations are also highlighted in the figures. EEJ = equatorial electrojet; IEF = interplanetary electric field.

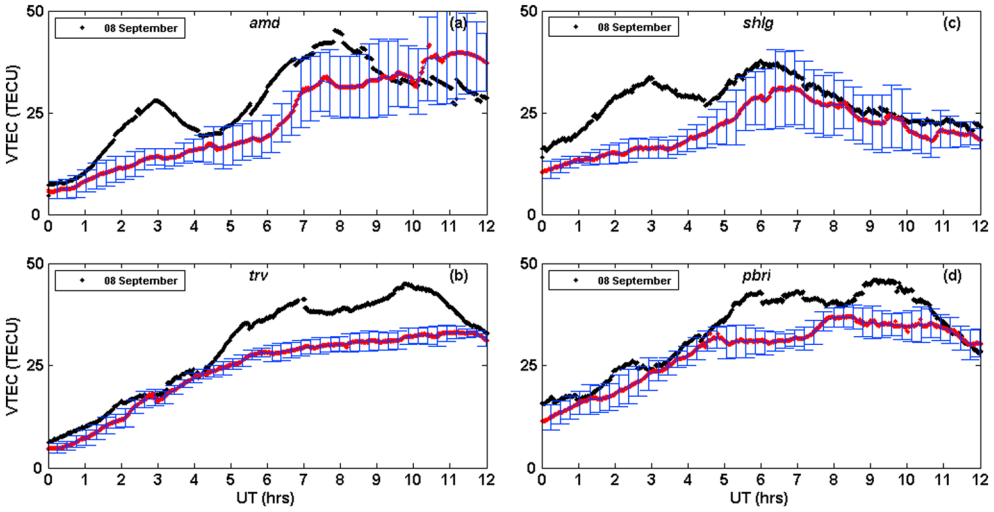

Figure 6. GPS-TEC variations as recorded at (a) *amd*, (b) *trv*, (c) *shlg*, and (d) *pbri* stations during 00:00 to 12:00 UT on 8 September 2017. Three quiet days' mean TEC along with the standard deviations for the same month are also presented in the figure.

12:00 UT on 8 September are shown separately in Figure S2 for better understanding of the storm activity. An intense flare of M8.1, occurred at ~07:40 UT, on 8 September coincided with the daytime over the Indian longitudes. The EEJ current enhanced by ~75% (over the preflare EEJ current value; Figure 4b). It has to be noted that SYM-H variations exhibited recovery of main phase step-I at this time. (Figures 1 and S2). The *F* region response was not clear to the flare of 8 September as observed through GPS-TEC. However, TEC (Figure 6) and EEJ current (Figure 5b) both responded considerably to the storm time electric fields on 8 September.

The EEJ current on 8 September showed large negative values at ~00:00 UT, which is around the dawn sector over the Indian longitudes (Figure 5b). The IEF_y showed very high positive value of ~19.78 mV/m at ~23:59 UT on 7 September, which reduced to 9.03 mV/m at ~00:41 UT on 8 September (Figure 1). The EEJ current again reduced between ~01:35 and ~02:30 UT and then gradually increased with time. The reduction in EEJ at ~01:35 UT coincided with a sharp IEF_y reduction. The interesting observation here is despite the IEF_y turning negative ~02:30 UT, the EEJ current steadily enhanced with time. Additionally, the SYM-H was also recovering around this time exhibiting the weakening of a ring current. The signatures of IEF_y enhancements, associated with the southward turning of IMF B_z, clearly appeared in EEJ current as various spikes, while the IEF_y changes associated with the northward turning of IMF B_z could not modulate the EEJ current to a significant extent on 8 September (Figure 5b).

Though the EEJ showed large negative values at ~00:00 UT on 8 September, the TEC at low latitude stations of *amd* and *shlg* (Figures 6a and 6c) showed significant enhancements at this epoch. However, the TEC at equatorial stations (near to the geomagnetic equator) of *tvm* and *pbri* did not vary much from that of the quiet day value (Figures 6b and 6d). The enhanced low latitude TEC started reducing at ~03:00 UT. This decrease in TEC continued till ~4:30 UT, before the initiation of the second TEC enhancements at low latitudes. It is important to note that equatorial TEC also exhibited gradual enhancements, over the quiet day value, around this time. The observed simultaneous TEC enhancements started to recover as observed from all GPS receiver stations. However, the TEC at equatorial stations showed another rise after this, while the TEC at low latitudes remained within the quiet day's TEC variability.

4. Discussion

The transient solar disturbances in terms of solar flares impart excess electromagnetic radiations in dayside. It is a known fact that incoming solar radiations ionize the dayside middle and upper atmosphere and generate partially ionized region, that is, ionosphere, within it. The respective ionizing wavelengths vary with the atmospheric altitudes. The middle atmosphere (~100 km) mainly responds to the soft X-rays (0.1 to 17 nm), EUV

(91.1 to 102.7 nm), and Lyman-α (~102.6 nm), while the upper atmosphere (~150 km onward) get ionized majorly by EUV (17 to 91.1 nm) and produce, respectively, *E* and *F* regions of the ionosphere. More details on this could be found in Rishbeth and Garriot (1969). The magnitude of the flare induced additional ionization at respective altitudes depends on many factors such as the flare intensity, local time of the flare occurrence, and location of the solar active region over the solar disk from where flare emerges (e.g., Leonovich et al., 2010; Mendillo & Evans, 1974; Thome & Wagner, 1971; Tsurutani et al., 2005; Zhang et al., 2002, and references therein).

The solar X-ray emission is mainly from the corona, while the EUV gets emitted from the lower solar atmosphere. Since the origins of X-rays and EUV fluxes are from different altitudes on the Sun, the correlation between these two changes significantly with the movement of the respective solar active region over the Sun (e.g., Donnelly, 1976; Zhang et al., 2011, and references therein). Despite the fact that at the occurrence time of X9.3 flare on 6 September the Indian longitudes were in the evening sector, with higher solar zenith angle values (Figure 2b), effect of a large amount of X-ray flux from this intense flare was reflected as a huge rise in *E* region ionization over the Indian region. Although the EEJ current response to this flare was rather impressive, the TEC did not show very high degree of changes. Though TEC is an integrated quantity, the *F* region electron density has major contribution in manifesting TEC variations. Tsurutani et al. (2005) reported the TEC changes during the Halloween events and showed that the TEC was enhanced by ~25 TECU on 28 October, while the enhancements was ~5–7 TECU during other two flare events of 29 October and 4 November 2003. It is important to note that the 4 November flare is the largest flare with X28 class in the National Oceanic and Atmospheric Administration records, while the 28 October flare is listed as X17. They discussed this contrasting TEC behavior in terms of the center-to-limb distance of the solar active region during these events. In the present case, we have seen that active region 12673 is at location S09W42 away from the center. We attribute the flare time poor response of low latitude TEC, observed in the present study, to the center-to-limb distance of the 12673 active region. As mentioned, *F* region ionization is mainly controlled by the solar EUV radiation. Since the X9.3 flare was not a center event, it might witness the absorption of solar EUV in the lower solar atmosphere. However, as mentioned, the X-ray from the corona does not have any such absorption. It has to be noted that earlier studies (e.g., Tsurutani et al., 2004) speculated this based on the TEC variations but no observations on the ionospheric response to X-ray radiation were presented simultaneously. Thus, this study could be appreciated in explaining the varying degree of ionospheric *E* region and *F* region variability in terms of the center-to-limb distance of the solar active region using multiparametric observations.

It is also important to note that flare induced TEC variations were found to be absent from *shlg* and *pbri* GPS stations, while the similar were observed from the *amd* and *tvm* GPS stations. In Figure 2b, the solar zenith angle variations show that both *amd* and *tvm* were in the presunset sector on 6 September at ~11:53 UT, while the Sun was almost at horizon at *shlg* and *pbri* already entered into the postsunset sector. Therefore, TEC from *shlg* and *pbri* are not expected to show any flare induced variations on 6 September.

As mentioned earlier, the ionospheric response to the flare is highly subjective if geomagnetic disturbances are present simultaneously. In the present case, geomagnetic disturbances started on 6 September at around ~23:53 UT and the IEF_y variations were significant on 7 September, although SYM-H did not show any major intensification. Both M-class flares of 7 September were accompanied by IEF_y enhancements (shaded region in Figure 5a) associated with the intensification of southward IMF B_z. The IEF_y fluctuations driven by southward IMF B_z results in eastward electric field penetration during daytime and thus enhances the *E* region current (e.g., Bagiya et al., 2011, 2014; Hui et al., 2017, and references therein). Therefore, we suggest that the EEJ current variations during two M-class flares on 7 September contain contributions from both flare as well as eastward IEF_y penetration. The M2.4 class flare occurred at ~04:59 UT (Figure 5a) is not discussed here due to the unavailability of IEF_y estimation during this time.

The EEJ current variations on 8 September were largely affected by the storm time transient electric fields perturbations at low latitudes (Figure 5b). We suggest that the negative swing in EEJ current between ~00:00 and ~01:35 UT on 8 September are the combined effects of the reduced convection effects at low latitudes due to IEF_y reduction and the effects of developing ring current during the main phase (Figure S2). Since the ionospheric ambient conductivity remains very less around dawn, the intense ring current signatures in EEJ current are obvious. After exhibiting multiple enhancements associated with the eastward IEF_y

Table 2
Comparisons Between the Flares and Storm Time EEJ Current and TEC

	IEF_y	EEJ current		TEC	
Date/flare	Variations (yes/no)	Enhancement time UT (75°E LT)	Enhanced intensity	Enhancement time UT (observable GPS station)	Enhanced intensity
6 September (X9.3)	No	~11.92 (16:55)	~22.3 nT (~500%)	~11.93 (*amd*)	~2.59 (~7%)
7 September (M1.4)	Yes	~9.88 (14:53)	~3.6 nT (~20%)	—	—
7 September (M7.3)	Yes	~10.28 (15:17)	~14.2 nT (~110%)	—	—
8 September (M8.1)	Yes	~7.75 (12:45)	~13.4 nT (~75%)	—	—

penetrations (Figure 5b), EEJ current responded significantly to the M8.1 flare (Figure 4b and shaded region in Figure 5b). It is to be noted that IEF_y was negative at this time. This emphasize that the storm induced convection was reduced during this period. Therefore, we suggest that the increase in EEJ current at this time was triggered by the M8.1 flare.

Table 2 shows the comparisons between the observed ionospheric variations during 6 to 8 September for quick review of this study. As expected the larger and long durable EEJ current enhancements were observed during X9.3 flare on 6 September. Though this flare occurred in local evening hours when the ambient conductivity remains less in general, the induced excess ionization could enhance the EEJ current significantly. The M8.1 flare occurred around the local noon hours on 8 September, but its signatures in EEJ current were less in amplitude compared to the M7.3 flare, which occurred in local afternoon hours on 7 September. This is due to the fact that during M7.3 flare the IEF_y penetration was in direction of ambient ionospheric electric field, while such augmentation of the ambient field was absent on 8 September, and instead, it was a weakening overshielding field, which is expected to reduce the EEJ current. In addition, the effect of storm induced disturbance dynamo electric field (DDEF), which is westward in dayside and reduce the ambient electric field, could not be ruled out in reducing the EEJ current. The lesser EEJ current compared to that of the quiet days' mean at ~07:15 UT (Figure 5b) corroborates these facts. Despite this, the EEJ current responded significantly to the M8.1 flare on 8 September.

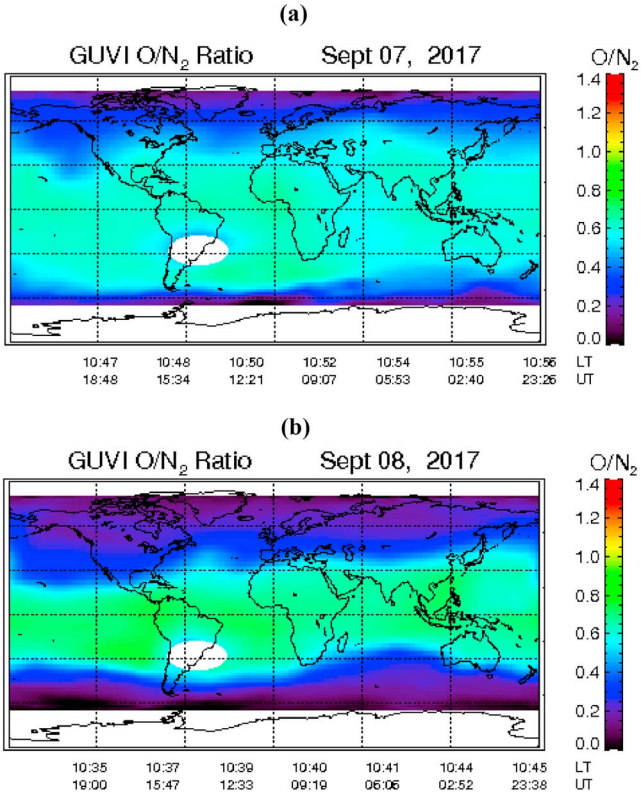

Figure 7. Thermospheric neutral compositions changes in terms of $[O/N_2]$ maps from GUVI on board Thermosphere Ionosphere Mesosphere Energetics and Dynamics satellite on (a) 7 September and (b) 8 September 2017.

The flare on 8 September could not produce any noticeable TEC changes, but the later varied significantly under the effects of the storm time electric fields. The low latitude TEC enhancements near the dawn hours, from *amd* and *shlg*, are attributed to the storm time prompt penetration electric field (PPEF) field (which raises the dayside ionospheric plasma to higher altitudes where the recombination rate is slow) in addition to the storm time neutral composition changes. The thermospheric neutral composition changes are, in general, understood as ratio of atomic oxygen (O) to molecular species (N_2 and O_2). The excess joule heating over high latitudes during a storm strengthens the upward vertical wind, which raises thermospheric molecular rich air to higher altitudes (Immel et al., 2001). The meridional wind along with the diurnal wind transports the enhanced thermospheric mean molecular mass (e.g., Prölss, 1980) toward mid and low latitudes (e.g., Bagiya et al., 2014; Fuller-Rowell et al., 1998; Roble et al., 1977, and references therein). The initial transport enhances the $[O/N_2]$ at low latitudes, which results into enhanced ionospheric density (through photoionisation of atomic oxygen), while the molecules that arrive later in time reduce electron density by enhancing the recombination rate with ambient N_2^+ and O_2^+ (e.g., Bagiya et al., 2011, 2014; Burns et al., 1991; Liou et al., 2005; Strickland et al., 2001). From the $[O/N_2]$ global maps by the Global Ultraviolet Imager (GUVI) on board Thermosphere Ionosphere Mesosphere Energetics and Dynamics (TIMED) satellite (e.g.,

Christensen et al., 2003; Paxton et al., 1999), it is realized that [O/N_2] ratio exhibited significant increase on 8 September in comparison to 7 September (Figure 7). This supports the observed TEC enhancements over the Indian low latitude stations. The equatorial TEC could not experience any such enhancements. For this behavior, we propose that the storm induced thermospheric neutrals changes could not arrive till the equator over this time. By keeping in view the limitations of GUVI maps in providing precise information on the compositional changes over a particular location, it is not feasible to show the difference in neutral composition changes over the equator and low latitudes in the present study.

The eastward PPEF ~3:30 UT led to the simultaneous enhancement of TEC over equatorial and low latitudes. The dayside westward DDEF penetration reduces the ionospheric electron density by lowering the *F* region heights to the area of higher recombination rate and also suppresses the evolution of equatorial ionization anomaly. The depression of equatorial ionization anomaly provides more ionization over the equatorial region than that of the low latitudes. Therefore, the second rise in the equatorial TEC (~08:30 UT) is attributed to the delayed DDEF penetration in addition to the weakening overshielding over the Indian longitudes during this period.

5. Summary

An exclusive case study on the combined effects of the solar flares and storm time electric fields over the low-latitude ionosphere during 6 to 8 September 2017 is presented here. This study could be appreciated in terms of delineating the effects of flare and storm time electric fields over the low latitude ionosphere. The main results could be summarized as follows:

1. Using multiparametric ionospheric observations, the different degree of *E* region and *F* region ionospheric enhancements is explained in terms of center-to-limb distance of the solar active region 12673 during the X9.3 flare on 6 September.
2. Low latitude TEC over the Indian longitudes clearly show the solar zenith angle dependence while responding to the X9.3 flare.
3. The storm time electric fields are observed to modulate the magnitudes of flare induced EEJ current enhancements during M7.3 and M8.1 flares on 7 and 8 September, respectively.
4. During the storm time PPEF, and in response to the subsequent neutral composition changes, the TEC over low latitude region enhanced significantly, while no such changes are seen over the equatorial region during the dawn hours, whereas the enhancements are observed at both equatorial and low latitudes during the prenoon hours.

This study is probably the first of its kind in demonstrating the modulations of flares effects over the low latitude ionosphere by the simultaneous prevailed geomagnetic disturbances.

Acknowledgments
M. S. B. duly acknowledges the staff at SGRC, Shillong, and MPGO Portblair for the continuous operation and maintenance of GNSS receivers. The authors are grateful to the NOAA GOES-15 team for the X-ray data, NASA SDO team for the EUV data and solar magnetogram images, OMNI team for the interplanetary and magnetospheric data, NASA, and MO&DA program for the GUVI data. The observatory and data analysis section of Indian Institute of Geomagnetism is duly acknowledged for providing EEJ data. The work of M. S. B., A. S., and D. H. are supported by Department of Science and Technology (DST), and the work of R. K. C. and S. V. T. are supported by Indian Space Research Organization, India. The EEJ and TEC data from Shillong and Portblair will be made available on www.iigm.res.in upon request at mala@iigs.iigm.res.in. The TEC data from Ahmedabad and Trivandrum will be made available on www.prl.res.in and on www.spl.gov.in upon request at dipu@prl.res.in and rajkumar_choudhary@vssc.gov.in, respectively.

References

Bagiya, M. S., Hazarika, R., Laskar, F. I., Sunda, S., Gurubaran, S., Chakrabarty, D., et al. (2014). Effects of prolonged southward interplanetary magnetic field on low-latitude ionospheric electron density. *Journal of Geophysical Research: Space Physics*, *119*, 5764–5776. https://doi.org/10.1002/2014JA020156

Bagiya, M. S., Iyer, K. N., Joshi, H. P., Thampi, S. V., Tsugawa, T., Ravindran, S., et al. (2011). Low-latitude ionospheric thermospheric response to storm time electrodynamical coupling between high and low latitudes. *Journal of Geophysical Research*, *116*, A01303. https://doi.org/10.1029/2010JA015845

Bagiya, M. S., Joshi, H. P., Iyer, K. N., Aggarwal, M., Ravindran, S., & Pathan, B. M. (2009). TEC variations during low solar activity period (2005–2007) near the equatorial ionospheric anomaly crest region in India. *Annales de Geophysique*, *27*(3), 1047–1057. https://doi.org/10.5194/angeo-27-1047-2009

Bagiya, M. S., Sunil, A. S., Chakrabarty, D., & Sunda, S. (2017). Salient features of the dayside low latitude ionospheric response to the main phase step-I of the 17 March 2015 geomagnetic storm. *Advances in Space Research*, *60*(8), 1827–1837. https://doi.org/10.1016/j.asr.2017.06.010

Bagiya, M. S., Vichare, G., Sinha, A. K., & Sripathi, S. (2018). On the nocturnal downward and westward equatorial ionospheric plasma drifts during the 17 March 2015 geomagnetic storm. *Journal of Geophysical Research: Space Physics*, *123*, 1618–1626. https://doi.org/10.1002/2017JA024703

Blanc, M., & Richmond, A. D. (1980). The ionospheric disturbance dynamo. *Journal of Geophysical Research*, *85*(A4), 1669–1688. https://doi.org/10.1029/JA085iA04p01669

Burns, A. G., Killeen, T. L., & Roble, R. G. (1991). A theoretical study of thermospheric composition perturbations during an impulsive geomagnetic storm. *Journal of Geophysical Research*, *96*(A8), 14,153–14,167. https://doi.org/10.1029/91JA00678

Chakrabarty, D., Bagiya, M. S., Thampi, S. V., Pathan, B. M., & Sekar, R. (2013). Signatures of moderate (M-class) and low (C and B class) intensity solar flares on the equatorial electrojet current: Case studies. *Journal of Atmospheric and Solar-Terrestrial Physics*, *105-106*, 170–180. https://doi.org/10.1016/j.jastp.2013.10.005

Christensen, A. B., Paxton, L. J., Avery, S., Craven, J., Crowley, G., Humm, D. C., et al. (2003). Initial observations with the Global Ultraviolet Imager (GUVI) in the NASA TIMED satellite mission. *Journal of Geophysical Research*, *108*(A12), 1451. https://doi.org/10.1029/2003JA009918

Davies, K. (1990). *Ionospheric radio*. London: Peter Peregrinus.

Donnelly, R. F. (1976). Empirical models of solar flare x-ray and EUV emissions for use in studying their *E* and *F* region effects. *Journal of Geophysical Research*, *81*(25), 4745–4753. https://doi.org/10.1029/JA081i025p04745

Fejer, B. G., Larsen, M. F., & Farley, D. T. (1983). Equatorial disturbance dynamo electric fields. *Geophysical Research Letters*, *10*(7), 537–540. https://doi.org/10.1029/GL010i007p00537

Fuller-Rowell, T. J., Codrescu, M. V., Roble, R. G., & Richmond, A. D. (1998). How does the thermosphere and ionosphere react to a geomagnetic storm? In B. T. Tsurutani, et al. (Eds.), *Magnetic storms, Geophysical Monograph Series* (Vol. 98, pp. 203–225). Washington, DC: American Geophysical Union.

Hanser, F. A., & Sellers, F. B. (1996). Design and calibration of the GOES-8 solar x-ray sensor: The XRS. *Proceedings of SPIE*, *2812*, 344–352. https://doi.org/10.1117/12.254082

Hui, D., Chakrabarty, D., Sekar, R., Reeves, G. D., Yoshikawa, A., & Shiokawa, K. (2017). Contribution of storm time substorms to the prompt electric field disturbances in the equatorial ionosphere. *Journal of Geophysical Research: Space Physics*, *122*, 5568–5578. https://doi.org/10.1002/2016JA023754

Immel, T. J., Crowley, G., Craven, J. D., & Roble, R. G. (2001). Dayside enhancements of thermospheric O/N_2 following magnetic storm onset. *Journal of Geophysical Research*, *106*(A8), 15,471–15,488. https://doi.org/10.1029/2000JA000096

Kamide, Y., & Kusano, K. (2015). No major solar flares but largest geomagnetic storm in the present solar cycle. *Space Weather*, *13*, 365–367. https://doi.org/10.1002/2015SW001213

Kelley, M. C., Makela, J. J., Chau, J. L., & Nicholls, M. J. (2003). Penetration of the solar wind electric field into the magnetosphere/ionosphere system. *Geophysical Research Letters*, *30*(4), 1158. https://doi.org/10.1029/2002GL016321

Klobuchar, J. (1986). Design and characteristics of the GPS ionospheric time-delay algorithm for single frequency users. In *Proceedings of PLANS'86—Position location and navigation symposium* (pp. 280–286). Nevada: Las Vegas.

Le, H., Liu, L., He, H., & Wan, W. (2011). Statistical analysis of solar EUV and X-ray flux enhancement induced by solar flares and its implication to upper atmosphere. *Journal of Geophysical Research*, *116*, A11301. https://doi.org/10.1029/2011JA016704

Leonovich, L. A., Tashchilin, A. V., & Portnyagina, O. Y. (2010). Dependence of the ionospheric response on the solar flare parameters based on the theoretical modeling and GPS data. *Geomagnetism and Aeronomy*, *50*(2), 201–210. https://doi.org/10.1134/S0016793210020076

Liou, K., Newell, P. T., Anderson, B. J., Zanetti, L., & Meng, C.-I. (2005). Neutral composition effects on ionospheric storms at middle and low latitudes. *Journal of Geophysical Research*, *110*, A05309. https://doi.org/10.1029/2004JA010840

Liu, J. Y., Lin, C. H., Chen, Y. I., Lin, Y. C., Fang, T. W., Chen, C. H., et al. (2006). Solar flare signatures of the ionospheric GPS total electron content. *Journal of Geophysical Research*, *111*, A05308. https://doi.org/10.1029/2005JA011306

Mahajan, K. K., Lodhi, N. K., & Upadhayaya, A. K. (2010). Observations of X-ray and EUV fluxes during X-class solar flares and response of upper ionosphere. *Journal of Geophysical Research*, *115*, A12330. https://doi.org/10.1029/2010JA015576

Mendillo, M., & Evans, J. V. (1974). Incoherent scatter observations of the ionospheric response to a large solar flare. *Radio Science*, *9*(2), 197–203. https://doi.org/10.1029/RS009i002p00197

Mendillo, M., Klobuchar, J. A., Fritz, R. B., da Rosa, A. V., Kersley, L., Yeh, K. C., et al. (1974). Behavior of the ionospheric *F* region during the greatest solar flare of August 7, 1972. *Journal of Geophysical Research*, *7*, 665–672. https://doi.org/10.1029/JA079i004p00665

Mitra, A. P. (1974). *Ionospheric effects of solar flares* (p. 294). NewYork: Springer. https://doi.org/10.1007/978-94-010-2231-6

Nagata, T. (1966). Solar flare effect on the geomagnetic field. *Journal of Geomagnetism and Geoelectricity*, *18*(2), 197–219. https://doi.org/10.5636/jgg.18.197

Nishida, A. (1968). Coherence of geomagnetic DP 2 fluctuations with interplanetary magnetic field variations. *Journal of Geophysical Research*, *73*(17), 5549–5559. https://doi.org/10.1029/JA073i017p05549

Paxton, L. J., Christensen, A. B., Humm, D. C., Ogorzalek, B. S., Thompson Pardoe, C., Morrison, D., et al. (1999). Global ultraviolet imager (GUVI): Measuring composition and energy inputs for the NASA Thermosphere Ionosphere Mesosphere Energetics and Dynamics (TIMED) mission. *Proceedings of SPIE The International Society for Optical Engineering*, *3756*, 265–276.

Pesnell, W. D., Thompson, B. J., & Chamberlin, P. C. (2012). The Solar Dynamics Observatory (SDO). *Solar Physics*, *275*(1-2), 3–15. https://doi.org/10.1007/s11207-011-9841-3

Prölss, G. W. (1980). Magnetic storm associated perturbations of the upper atmosphere: Recent results obtained by satellite-borne gas analyzers. *Reviews of Geophysics and Space Physics*, *18*(1), 183–202. https://doi.org/10.1029/RG018i001p00183

Prolss, G. W. (1997). Magnetic storm perturbations of the upper atmosphere. In B. T. Tsurutani, et al. (Eds.), *Magnetic storms, Geophysical Monograph Series* (Vol. 98, pp. 227–241). Washington, DC: American Geophysical Union.

Raja Rao, K. S., & Panduranga Rao, M. (1963). On the location of ionospheric current system causing geomagnetic solar flare effects. *Journal of the Atmospheric Sciences*, *20*(6), 498–501. https://doi.org/10.1175/1520-0469(1963)020<0498:OTLOTI>2.0.CO;2

Rama Rao, P. V. S., Gopi Krishna, S., Niranjan, K., & Prasad, D. S. V. V. D. (2006). Temporal and spatial variations in TEC using simultaneous measurements from the Indian GPS network of receivers during the low solar activity period of 2004–2005. *Annales de Geophysique*, *24*(12), 3279–3292. https://doi.org/10.5194/angeo-24-3279-2006

Rastogi, R. G., & Klobuchar, J. A. (1990). Ionospheric electron content within the equatorial F_2 layer anomaly belt. *Journal of Geophysical Research*, *95*(A11), 19,045–19,052. https://doi.org/10.1029/JA095iA11p19045

Rastogi, R. G., Pathan, B. M., Rao, D. R. K., Sastry, T. S., & Sastri, J. H. (1999). Solar flare effects on the geomagnetic elements during normal and counter electrojet periods. *Earth, Planets and Space*, *51*, 947–957.

Richmond, A. D., & Venkateswaran, S. V. (1971). Geomagnetic crochets and associated ionospheric current systems. *Radio Science*, *6*, 139–164.

Rishbeth, H., & Garriot, O. K. (1969). *Introduction to ionospheric physics*. New York: Academic Press.

Roble, R. G., Dickinson, R. E., & Ridley, E. C. (1977). Seasonal and solar cycle variations in the zonal mean circulation in the thermosphere. *Journal of Geophysical Research*, *82*(35), 5493–5504. https://doi.org/10.1029/JA082i035p05493

Strickland, D. J., Daniell, R. E. Jr., & Craven, J. D. (2001). Negative ionospheric storm coincident with DE 1-observed thermospheric disturbance on October 14, 1981. *Journal of Geophysical Research*, *106*(A10), 21,049–21,062. https://doi.org/10.1029/2000JA000209

Thome, G. D., & Wagner, L. S. (1971). Electron density enhancements in the *E* and *F* regions of the ionosphere during solar flares. *Journal of Geophysical Research*, *76*(28), 6883–6895. https://doi.org/10.1029/JA076i028p06883

Tsurutani, B. T., Judge, D. L., Guarnieri, F. L., Gangopadhyay, P., Jones, A. R., Nuttall, J., et al. (2005). The October 28, 2003 extreme EUY solar flare and resultant extreme ionospheric effects: Comparison to other Halloween events and the Bastille Day event. *Geophysical Research Letters*, *32*, L03S09. https://doi.org/10.1029/2004GL021475

Tsurutani, B. T., Mannucci, A., Iijima, B., Abdu, M. A., Sobral, J. H. A., Gonzalez, W., et al. (2004). Global dayside ionospheric uplift and enhancement associated with interplanetary electric field. *Journal of Geophysical Research*, *109*, A08302. https://doi.org/10.1029/2003JA010342

Zhang, D. H., Mo, X. H., Cai, L., Zhang, W., Feng, M., Hao, Y. Q., & Xiao, Z. (2011). Impact factor for the ionospheric total electron content response to solar flare irradiation. *Journal of Geophysical Research*, *116*, A04311. https://doi.org/10.1029/2010JA016089

Zhang, D. H., Xiao, Z., Igarashi, K., & Ma, G. Y. (2002). GPS derived ionospheric total electron content response to a solar flare that occurred on 14 July 2000. *Radio Science*, *37*(5), 1086. https://doi.org/10.1029/2001RS002542